



Dynamical regimes and clustering of small neutrally buoyant inertial particles in stably stratified turbulence

Christian Reartes  and Pablo D. Mininni 

*Universidad de Buenos Aires, Facultad de Ciencias Exactas y Naturales,
Departamento de Física, Ciudad Universitaria, 1428 Buenos Aires, Argentina
and CONICET–Universidad de Buenos Aires, Instituto de Física Interdisciplinaria y Aplicada (INFINA),
Ciudad Universitaria, 1428 Buenos Aires, Argentina*



(Received 6 December 2022; accepted 26 April 2023; published 16 May 2023)

Inertial particles in stably stratified flows play a fundamental role in geophysics, from the dynamics of nutrients in the ocean to the dispersion of pollutants in the atmosphere. We consider the Maxey-Riley equation for small neutrally buoyant inertial particles in the Boussinesq approximation and discuss its limits of validity. The main motivation is the study of phytoplankton and oceanic particles in turbulent flows. We show that particles behave as forced damped oscillators, with different regimes depending on the particles Stokes number and the fluid Brunt-Väisälä frequency. Using direct numerical simulations we study their dynamics and show that small neutrally buoyant particles in these flows tend to cluster in regions of low local vorticity. The particles, albeit small, behave fundamentally differently than tracers.

DOI: [10.1103/PhysRevFluids.8.054501](https://doi.org/10.1103/PhysRevFluids.8.054501)

I. INTRODUCTION

Dispersion of inertial particles by turbulent flows plays a fundamental role in many geophysical systems, from cloud formation and the dispersion of pollutants in the atmosphere to the dynamics of plankton in the ocean [1–4]. In spite of their interest, the dynamics of particles in these systems is poorly understood. We know the equations of motion of small particles (i.e., such that the Reynolds number at the particle scale is much smaller than unity [5]), and in recent years experiments [6] and particle-resolved simulations [7] have provided valuable insights into particles' dynamics in other regimes. However, particle transport problems in geophysics necessarily require reduced models that simplify the physics, as even in the cases in which a simulation can be done resolving a broad range of scales, an ensemble of runs to get statistical information becomes rapidly unfeasible. This has resulted, e.g., for stratified flows as in the oceans and the atmosphere, in the modeling of inertial particles simply as Lagrangian tracers [8] or using simplified models [9,10].

Modeling geophysical flows pose other challenges, even without particles. Stably stratified turbulence is anisotropic, and as a result it is fundamentally different from homogeneous isotropic turbulence (HIT) [11–13]. In these flows stratification reduces the vertical velocity, confining the flow into a quasihorizontal layered motion, also generating vertically sheared horizontal winds (VSHWs) with strong vertical variability [14]. The stratification results in a restoring force, allowing for the excitation of waves that can coexist with the turbulence. The spectral scaling of stably stratified turbulence is also different than in HIT, with a rich behavior depending on the scale considered, and on many dimensionless parameters. In broad terms, stably stratified turbulence displays an anisotropic subrange with a direct energy cascade between the buoyancy and Ozmidov scales [15,16]. Studies also indicate that larger-scale quasihorizontal motions can be a continuous source of small scale turbulence as long as the local Reynolds number does not drop below a threshold [17].

Many recent studies have considered stably stratified flows from a Lagrangian perspective (i.e., by considering tracers, or particles with inertia, that are transported by such flows). As an example, the Lagrangian transport of tracers in stably stratified turbulence was studied in Refs. [18,19]. However, the general equations of motion for inertial particles submerged in turbulent flows are not clear. For very small particles the Maxey-Riley approximation provides a set of equations for their dynamics [5]. As particles become larger, Basset-Boussinesq and Faxen corrections become relevant, but for even larger particles such perturbative expansion breaks down. The case of stably stratified turbulence is simpler than HIT in some way: most particles and aerosols are much smaller than the dissipation scale, and thus the Maxey-Riley approximation should hold (except for, e.g., large rain droplets in clouds, or snowflakes). But even in this regime, the derivation of the equations requires certain approximations and depend on the form of the equations for the fluid [20,21].

A fundamental feature of particles in homogeneous and isotropic turbulent flows is their preferential concentration. Turbulence sometimes separates the particles instead of mixing them. The detailed mechanisms by which turbulence affects particle motions are still unclear. In the homogeneous and isotropic case, and for the average concentration, the main mechanisms behind the well known case of heavy particles clustering are centrifugal expulsion [5] and the sweep-stick mechanism [22]. Evidence of preferential concentration of heavy particles in laboratory experiments and numerical simulations was reported, e.g., in Ref. [23]. Multiscale flow effects may be also relevant [24,25], and the role of other effects in preferential concentration, such as finite particle radius or the effect of large-scale flows, are still unclear [26–28]. However, it is important to note that not all particles cluster in homogeneous and isotropic turbulence. While small heavy particles do cluster, experimental [27] and numerical [29] evidence indicate that small neutrally buoyant particles (the case that will be of interest in this work) in the isotropic and homogeneous case sample turbulence homogeneously and do not cluster. In the particular case of stratified turbulence it has been shown that different inertial particles cluster for a wide range of parameters [21]. Vertical confinement caused by density stratification produces strong fractal clustering at isopycnic surfaces. Clustering was found to depend on a single parameter, the combination of the Stokes time τ_p of the particles and the Brunt-Väisälä frequency of the flow. In the limit of small τ_p (i.e., small inertia), clustering was found to increase monotonically with τ_p [21].

In this work we consider the Maxey-Riley model for small inertial particles [5], from which we derive an equation for the dynamics of inertial particles in stably stratified flows. The main motivation is the case of oceanic flows in which particles, such as phytoplankton, seaweed, and other oceanic particles, are transported by the turbulent flow [30–33]; other applications include particles with small or negligible settling velocity in atmospheric flows such as those found in the stratosphere [34]. We perform direct numerical simulations of the Boussinesq equations for the fluid, together with the Maxey-Riley equation for one million particles. We derive a simple model for the particles vertical displacement, and compare the model with the simulations to show that particles behave as forced damped oscillators with different regimes depending on the Stokes and Froude numbers. We characterize the dependence of the stratification-induced vertical confinement of the particles on these two parameters. Finally, we study the formation of clusters using Voronoi tessellation, and show that particles in stably stratified flows tend to accumulate in regions with low vorticity, at least for the range of parameters considered in the present study.

II. EQUATIONS OF MOTION

In this work we solve numerically the incompressible Boussinesq equations for the velocity \mathbf{u} and for mass density fluctuations ρ' ,

$$\partial_t \mathbf{u} + \mathbf{u} \cdot \nabla \mathbf{u} = -\nabla(p/\rho_0) - (g/\rho_0)\rho' \hat{\mathbf{z}} + \nu \nabla^2 \mathbf{u} + \mathbf{f}, \quad (1)$$

$$\partial_t \rho' + \mathbf{u} \cdot \nabla \rho' = (\rho_0 N^2/g) \mathbf{u} \cdot \hat{\mathbf{z}} + \kappa \nabla^2 \rho', \quad (2)$$

$$\nabla \cdot \mathbf{u} = 0, \quad (3)$$

where p is the correction to the hydrostatic pressure, ν is the kinematic viscosity, \mathbf{f} is an external mechanical forcing, N is the Brunt-Väisälä frequency (which in this approximation sets the stratification), and κ is the diffusivity. In terms of the background density gradient, the Brunt-Väisälä frequency is $N^2 = -(g/\rho_0)(d\bar{\rho}/dz)$, with $d\bar{\rho}/dz$ the imposed (linear) background stratification, and ρ_0 the mean fluid density. We write scaled density fluctuations ζ in units of velocity by defining $\zeta = g\rho'/(\rho_0N)$. All quantities are then made dimensionless using a characteristic length L_0 and a characteristic velocity U_0 in the domain, resulting in

$$\partial_t \mathbf{u} + \mathbf{u} \cdot \nabla \mathbf{u} = -\nabla(p/\rho_0) - N\zeta \hat{z} + \nu \nabla^2 \mathbf{u} + \mathbf{f}, \quad (4)$$

$$\partial_t \zeta + \mathbf{u} \cdot \nabla \zeta = N\mathbf{u} \cdot \hat{z} + \kappa \nabla^2 \zeta. \quad (5)$$

Inertial particles are modeled using the Maxey-Riley model, but we consider an approximation consistent with those made to obtain the Boussinesq equations, in addition to assuming that the typical length over which the velocity field changes appreciably is much larger than the particle radius a . Under the latter hypothesis the Faxén terms are negligible. Under the Boussinesq approximation for a stratified flow, Eqs. (4) and (5) are obtained from the Navier-Stokes equations after neglecting all density fluctuations except for those in the buoyancy force. Thus, for the dynamics of the particles we also consider the density and the mass of the fluid displaced by the particles in terms of their mean values, respectively, $\rho_f \approx \bar{\rho}_f = \rho_0$ and $m_f \approx \bar{m}_f = \rho_0 V_p$ (where V_p is the volume of the particles), except in the gravity term. In that term we consider the entire fluid density dependence, $\rho_f = \rho_0 + d\bar{\rho}/dz(z - z_0) + \rho'$, for a linear background density profile. As the flow is stably stratified, $d\bar{\rho}/dz < 0$. Under these approximations the equation for the particles results in

$$\begin{aligned} \dot{\mathbf{v}} \left(1 + \frac{1}{2} \frac{\bar{m}_f}{m_p} \right) &= \frac{6\pi a \bar{\rho}_f \nu}{m_p} [\mathbf{u}(\mathbf{x}, t) - \mathbf{v}(t)] + \frac{3}{2} \frac{\bar{m}_f}{m_p} \frac{D}{Dt} \mathbf{u}(\mathbf{x}, t) \\ &- g \left[1 - \frac{1}{\rho_p} \left(\rho_0 + \frac{d\bar{\rho}}{dz} (z - z_0) + \rho' \right) \right] \hat{z} + \frac{6\pi a^2 \bar{\rho}_f \nu}{m_p} \int_0^t \frac{d}{d\tau} [\mathbf{u}(\mathbf{x}, \tau) - \mathbf{v}(\tau)] \\ &\times \frac{d\tau}{\sqrt{\pi \nu (t - \tau)}}, \end{aligned} \quad (6)$$

where \mathbf{x} is the particle position, \mathbf{v} is the particle velocity, $\mathbf{u}(\mathbf{x}, t)$ is the fluid velocity at the particle position, D/Dt is the Lagrangian derivative, d/dt is the time derivative following the particle trajectory, and ρ_p is the particle mass density (particles are assumed to be spherical). For a fluid at rest, note particles will be at equilibrium (i.e., neutrally buoyant) when $1 - \rho_f/\rho_p = 0$, and that there is some freedom on how ρ_0 and z_0 are chosen. In particular, without loss of generality we can choose $\rho_p = \rho_0$, such that particles are neutrally buoyant at $z = z_0$ in the absence of density fluctuations.

Multiplying and dividing the buoyancy term in Eq. (6) by ρ_0 , we have

$$\begin{aligned} \dot{\mathbf{v}} \left(1 + \frac{1}{2} \frac{\bar{m}_f}{m_p} \right) &= \frac{6\pi a \bar{\rho}_f \nu}{m_p} [\mathbf{u}(\mathbf{x}, t) - \mathbf{v}(t)] + \frac{3}{2} \frac{\bar{m}_f}{m_p} \frac{D}{Dt} \mathbf{u}(\mathbf{x}, t) \\ &- \frac{\rho_0}{\rho_p} \left[\frac{g}{\rho_0} \frac{d\bar{\rho}}{dz} (z - z_0) + g \frac{\rho'}{\rho_0} \right] \hat{z} + \frac{6\pi a^2 \bar{\rho}_f \nu}{m_p} \int_0^t \frac{d}{d\tau} [\mathbf{u}(\mathbf{x}, \tau) - \mathbf{v}(\tau)] \frac{d\tau}{\sqrt{\pi \nu (t - \tau)}}, \end{aligned} \quad (7)$$

where the first term inside the brackets in the buoyancy is $-N^2$, while the second term is $N\zeta$. Reordering the terms in the equation and using dimensionless units, we finally obtain

$$\dot{\mathbf{v}} = \frac{1}{\tau_p} [\mathbf{u}(\mathbf{x}, t) - \mathbf{v}(t)] - \frac{2}{3} N [N(z - z_0) - \zeta] \hat{z} + \frac{D}{Dt} \mathbf{u}(\mathbf{x}, t) + \sqrt{\frac{3}{\pi \tau_p}} \int_0^t \frac{d}{d\tau} [\mathbf{u}(\mathbf{x}, \tau) - \mathbf{v}(\tau)] \frac{d\tau}{\sqrt{t - \tau}}, \quad (8)$$

where the particle relaxation time is $\tau_p = (m_p + \bar{m}_f/2)/(6\pi a\bar{\rho}_f\nu)$. For a spherical particle $\tau_p = a^2/(3\nu)$, with $\gamma = \bar{m}_f/m_p = 1$. We define the Stokes number as $St = \tau_p/\tau_\eta$, where $\tau_\eta = (\nu/\varepsilon)^{1/2}$ is the Kolmogorov timescale and ε is the fluid kinetic energy dissipation rate. Note that any other choice for $\gamma = \bar{m}_f/m_p$ is equivalent to changing the reference value ρ_0 , and results in the particles being neutrally buoyant at a different height (or equivalently, it results in a redefinition of z_0).

III. NUMERICAL SET UP

Besides the Stokes number that characterizes the particles, Eqs. (4) and (5) have two controlling parameters for the fluid, the Reynolds and Froude numbers,

$$\text{Re} = \frac{LU}{\nu}, \quad \text{Fr} = \frac{U}{LN}, \quad (9)$$

where $L = \pi/(2u^2) \int E(k)/k dk$ and $U = \langle |\mathbf{u}|^2 \rangle^{1/2}$ are, respectively, the characteristic Eulerian integral length and the root-mean-square (r.m.s.) flow velocity [with $E(k)$ the isotropic kinetic energy spectrum, and $u^2 = U^2/3$]. Using these parameters we can also define the buoyancy Reynolds number

$$\text{Rb} = \text{Re Fr}^2, \quad (10)$$

which provides an estimation of how turbulent the flow is at the buoyancy scale $L_b = U/N$, and plays an important role characterizing the flow dynamics. For $\text{Rb} \gg 1$ strong stratified turbulence can develop, while for $\text{Rb} \ll 1$ turbulent motions are strongly damped by viscosity. Although geophysical flows typically have large Rb (observations in the ocean thermocline yield $\text{Rb} \approx 10^2\text{--}10^3$ [35]), computational power limits the values of Rb that can be directly simulated. Considering numerical limitations here we study flows with Rb from 13 to 76. Previous studies show that $\text{Rb} > 10$ suffices to attain sufficiently strong turbulence in the small scales [36]. The Ozmidov scale, $L_{\text{oz}} = 2\pi/k_{\text{oz}}$ (with $k_{\text{oz}} = \sqrt{N^3/\varepsilon}$), also plays an important role in the dynamics, as for scales sufficiently small compared with L_{oz} the flow is expected to recover isotropy. For $\text{Rb} > 1$, L_{oz} is larger than the Kolmogorov dissipation scale η , and quasiisotropic turbulent transport can be expected to take place at the smallest dynamical scales in the flow.

Setting these parameters and choosing the forcing prescribes the numerical simulations. For the forcing we use Taylor-Green forcing [37], which is a two-velocity components forcing that generates pairs of large-scale counter-rotating eddies perpendicular to the stratification, with a shear layer in between. Its expression is given by

$$\mathbf{f} = f_0[\sin(k_fx)\cos(k_fy)\cos(k_fz)\hat{\mathbf{x}} - \cos(k_fx)\sin(k_fy)\cos(k_fz)\hat{\mathbf{y}}], \quad (11)$$

where f_0 is the amplitude of the forcing, $k_f = 1/L_0$ is the forcing wave number, and L_0 a unit length. This flow has been used before to study stratified turbulence [17,19]. In the stratified case it generates a large-scale circulation with VSHWs (i.e., with a nonzero mean horizontal velocity) only in the shear layer between the large-scale Taylor-Green vortices (see Ref. [38] for a movie of the development of the mean horizontal wind in this layer). Note that this forcing is constant in time, thus introducing no new timescale in the system. The Froude number in Eq. (9) can be considered as the ratio between the resulting frequency of the large-scale eddies and the Brunt-Väisälä frequency.

The Boussinesq fluid equations, Eqs. (4) and (5), were solved in a triply periodic domain using a parallelized and fully dealiased pseudospectral method, and a second-order Runge-Kutta scheme for time integration [39]. The equation for the particles, Eq. (8), was solved using third-order spline interpolation to estimate the forces at the particles positions, and with a second-order Runge-Kutta method for the time evolution [40].

We performed several direct numerical simulations of the Boussinesq equations with different Froude numbers, using a spatial resolution of $N_x = N_y = 768$ and $N_z = 192$ grid points, in a triple periodic domain of length $L_x = L_y = 2\pi L_0$ in the horizontal directions and $L_z = H = \pi L_0/2$ in the vertical direction. Three different Brun-Väisälä frequencies are considered (times are measured in

TABLE I. Relevant parameters of the fluid simulations. NT_0 is the Brunt-Väisälä frequency in units of $T_0^{-1} = U_0/L_0$, Fr is the Froude number, Re is the Reynolds number, Rb is the buoyancy Reynolds number, L is the flow integral scale, η is the Kolmogorov scale, L_b is buoyancy length, and L_{Oz} is the Ozmidov length scale. All lengths are in units of the unit length L_0 .

Run	NT_0	Fr	Re	Rb	L/L_0	η/L_0	L_b/L_0	L_{Oz}/L_0
N04	4	0.20	1900	76	1.27	0.0065	0.25	0.30
N08	8	0.12	1700	24	1.07	0.0065	0.13	0.10
N12	12	0.09	1600	13	1.00	0.0065	0.09	0.06

units of a unit turnover time $T_0 = L_0/U_0$, with U_0 a unit velocity, see Table I for all the relevant fluid parameters). All simulations have a Prandtl number $\text{Pr} = \nu/\kappa = 1$ (which should be considered as a turbulent Prandtl number [41,42]). The kinematic viscosity is chosen so that the Kolmogorov scale $\eta = (\nu^3/\varepsilon)^{1/4} \approx 0.0065L_0$ is well resolved, where the kinetic energy dissipation rate is computed as $\varepsilon = \nu\langle|\boldsymbol{\omega}|^2\rangle$ and $\boldsymbol{\omega} = \nabla \times \mathbf{u}$ is the vorticity. This results in $\kappa\eta \approx 1.6$, where $\kappa = N_x/(3L_0)$ is the maximum resolved wave number, corresponding to spatially well resolved simulations [43,44].

Once the flows in these simulations have reached a turbulent steady state (we integrated the system for 50 large-scale turnover times), we randomly distributed particles in a horizontal strip of width $H/5$ centered around $z_0 = H/2$ (i.e., at the height of the shear layer of the Taylor-Green flow), with initial velocities equal to the fluid velocity at the center of each particle. The dynamics of the particles neglected the last term in Eq. (8) (i.e., the Basset-Boussinesq history term). However, that term was computed *a posteriori* to estimate its relevance in the dynamics. Particles were one-way coupled, and thus they can be considered as test particles: they do not collide, and their volume fraction is irrelevant for the flow dynamics. Thus, the number of particles should be considered solely as a way to improve the statistics. In each simulation in Table I we added three sets of different particles with 10^6 particles each, with three different values of τ_p (or equivalently, different Stokes numbers), resulting in a total of nine datasets of particles with different values of Fr and St. Particles were integrated for almost 20 large-scale turnover times. Table II lists the relevant parameters of all these datasets, including the particle Reynolds number $\text{Re}_p = a|\mathbf{u} - \mathbf{v}|/\nu$ in each case, which in our simulations takes values from 0.1 to 4.2. Note that Tables I and II should be read together, as we can have, e.g., particles with $\text{St} = 0.3$ in a flow with $N = 4/T_0$, or the same particles in a flow with $N = 8/T_0$ or $12/T_0$. As a rule, the Basset-Boussinesq force is smaller than the drag force in all simulations except in the cases with $\text{St} = 3$; for those particles the Basset-Boussinesq history term becomes comparable to the Stokes drag (even though both terms are smaller than buoyancy and added mass forces), and Re_p also becomes larger than unity. Thus, studying particles with larger St would require taking the Basset-Boussinesq force into account (see, e.g., Ref. [20]), as well as other corrections to the Maxey-Riley equation.

To put these dimensionless values in context, we consider the case of oceanic flows. The Froude number in the ocean varies from $\approx 10^{-2}$ for the large-scale ocean circulation, to 10^{-1} at vertical scales of the order of $H = 1$ km [45]. At the latter case the typical Brunt-Väisälä

TABLE II. Relevant parameters of the particles in all simulations. St is the Stokes number, τ_p/T_0 is the Stokes time in units of T_0 , a/η is the particle radius in units of the Kolmogorov scale, and Re_p are the respective particles Reynolds numbers for all the Brunt-Väisälä frequencies.

Label	St	τ_p/T_0	a/η	Re_p		
				$NT_0 = 4$	$NT_0 = 8$	$NT_0 = 12$
St03	0.3	0.024	1.08	0.2	0.2	0.1
St1	1	0.076	1.85	0.7	0.5	0.2
St3	3	0.235	3.38	4.2	2.7	1.6

frequency is $N \approx 10^{-3} \text{ s}^{-1}$. Using these length and timescales to put dimensions in simulation N08, r.m.s. horizontal velocities result $\approx 0.08 \text{ m s}^{-1}$, comparable to typical velocities in the ocean of 0.1 m s^{-1} [45]. Of course, the separation of scales in the simulations is smaller than in realistic oceanic flows. As a result, for the particles we compare their size and timescales with those of the smallest dynamical scales in the system. Oceanic particles in the lower mixed layer or in the upper seasonal thermocline have a Kolmogorov timescale $\tau_\eta \approx 3 \text{ s}$, resulting in Stokes numbers between $\text{St} \approx 0.3$ to 3, corresponding to variations in particle radius between 1 to 3 mm [31] (to be compared against Kolmogorov dissipation scales between 0.1 and 10 mm [46]). Also, for oceanic particles in this size range the mass ratio is $\gamma \approx 1.003$ [30]. In the case of phytoplankton (and, in particular, of nanoplankton and microplankton) their typical sizes vary between 2 to 200 microns [32]. Taking into account that they are found in the mixed layer, the Stokes number varies between $\text{St} \approx 10^{-5}$ to 10^{-1} while the ratio a/η varies in the range of 0.02 to 2. Seaweed provides another example for which modified Maxey-Riley equations (in this case, using effective parameters) have been used for their modeling (see Refs. [10,33]).

Before proceeding to the detailed analysis of the results, the reader can find as Supplemental Material [38] several movies that provide a first qualitative description of the system dynamics. Stratified turbulence spontaneously develops layers with strong horizontal winds and smaller vertical velocities, this can be seen in a movie that shows the early time evolution of the flow. Once particles are added they move horizontally, advected by the horizontal winds, and in comparison they displace less vertically. The vertical displacement can be seen in a movie that shows the vertical dispersion of particles with different St in the flow with $\text{Fr} = 0.20$. In this movie, vertical motions can be qualitatively associated to a combination of internal gravity waves and turbulent eddies (see Secs. IV and V for details). Particles with smaller St are trapped more frequently by eddies, increasing their vertical dispersion, while particles with larger St tend to oscillate around the equilibrium. The horizontal displacement of the particles is shown in another movie of particles with $\text{St} = 1$ and $\text{Fr} = 0.12$. Not only the particles are carried by the horizontal winds and eddies, but they also cluster, generating regions in which the particles accumulate strongly. This phenomenon of preferential concentration of particles will be discussed in detail in Sec. VI.

IV. SPECTRA AND PARTICLE VERTICAL DISPLACEMENT MODEL

We first study the power spectrum of the particles' vertical velocity. Figure 1 shows this spectrum for different values of the Froude and Stokes numbers; frequencies are normalized by the Brunt-Väisälä frequency of the carrier flow. A peak is always present at $\omega \approx N$, and for small Fr a second peak at lower frequencies is observed. Its position and amplitude depends on Fr , while its amplitude depends only weakly on St . The peak at $\omega \approx N$ is followed for larger frequencies by a steep spectrum, and decays slowly for smaller frequencies.

The origin of the two peaks in the spectra can be explained by a simple model derived from the equation of motion of the particles. Equation (8) can be rewritten in terms of the particles' vertical position z using that $\dot{z} = v_z$ and $\ddot{z} = \dot{v}_z$, resulting in

$$\ddot{z} = \frac{1}{\tau_p} [u_z(\mathbf{x}, t) - \dot{z}] - \frac{2}{3} N [N(z - z_0) - \zeta] + \frac{D}{Dt} u_z(\mathbf{x}, t), \quad (12)$$

where the Basset-Boussinesq history force was neglected. Rearranging terms in Eq. (12) we arrive at the following expression,

$$\ddot{z} + \frac{1}{\tau_p} \dot{z} + \frac{2}{3} N^2 z = \ddot{z}_{\text{wav}} + \frac{1}{\tau_p} \dot{z}_{\text{wav}} + \frac{2}{3} N^2 z_{\text{wav}}, \quad (13)$$

where we assumed that vertical displacements of fluid elements are caused by internal gravity waves, and thus we defined $z_{\text{wav}} = z_0 + \zeta/N$, $\dot{z}_{\text{wav}} = u_z(\mathbf{x}, t)$, and $\ddot{z}_{\text{wav}} = Du_z/Dt$. Equation (13) is the equation of a driven damped oscillator with system frequency $\sqrt{2/3}N$, damping constant $(2\tau_p)^{-1}$, and forcing $f_{\text{wav}} = \ddot{z}_{\text{wav}} + \dot{z}_{\text{wav}}/\tau_p + 2N^2 z_{\text{wav}}/3$. The pulsation of the damped system is

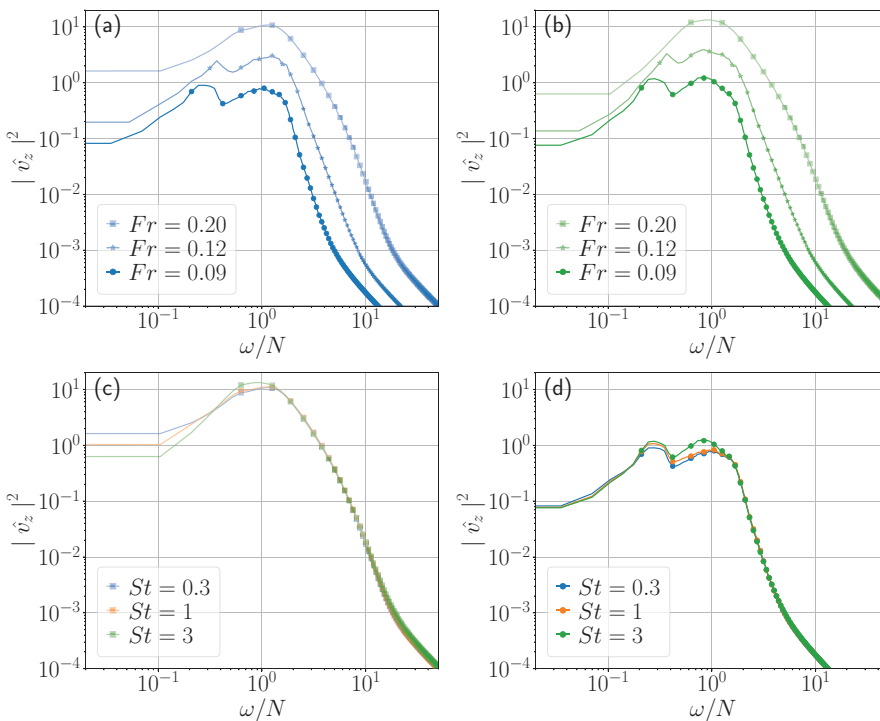


FIG. 1. Power spectra of the particles' vertical velocity, for different values of the Froude and Stokes numbers. (a) $St = 0.3$ and (b) $St = 3$, for different Fr (indicated in the insets). Power decreases with increasing stratification. (c) $Fr = 0.20$ and (d) $Fr = 0.09$, for different St (indicated in the insets). The value of St has a small effect in the amplitude of the main peak.

$\Omega^2 = 2N^2/3 - (2\tau_p)^{-2}$. For particles with small inertia this results in an over-damped system (i.e., $\Omega^2 < 0$) and when perturbed, particles slowly decay to the equilibrium position following fluid elements. Particles with large inertia result instead in weak damping ($\Omega^2 > 0$), and perturbed particles oscillate around the equilibrium as they decay, only weakly following the fluid elements. Indeed, the dependence of the frequency of oscillation with τ_p is in qualitative agreement with the results in Figs. 1(c) and 1(d); note that as St increases, the main peak of the spectrum moves from $\omega \approx N$ to lower frequencies (as a reference, for $St = 3$ Eq. (13) yields a frequency $\Omega \approx 0.82N$).

Equation (13) can be integrated numerically if f_{wav} is prescribed. As we do not know the precise evolution of u_z as seen by each particle, we assume u_z is a random colored process. The spectrum of the fluid vertical velocity in many stably stratified flows is compatible with the Garrett-Munk spectrum, as observed in oceanic observations [47] and in numerical simulations [19]. This is a flat power spectrum for frequencies $\omega \leq N$, resulting from the superposition of internal gravity waves, followed by a power law decay for $\omega > N$. Thus, we consider a random superposition of oscillators of the form

$$\dot{z}_{\text{wav}} = u_0 \text{Re} \left(\sum_{\omega}^{N \geq \omega > N/4} \frac{e^{i\omega t + \phi_\omega}}{\omega} + \sum_{\omega}^{\omega > N} N \frac{e^{i\omega t + \phi_\omega}}{\omega^2} \right), \quad (14)$$

where ϕ_ω are random phases (note that, as we are interested only in vertical motions, the dependence of traveling waves on x and y can be ignored or absorbed into the random phases), and u_0 is an amplitude chosen so that \dot{z}_{wav} has the same r.m.s. value as that of u_z in the numerical simulations. The power spectrum of \dot{z}_{wav} that results is compatible with oceanic observations of the Garret-Munk

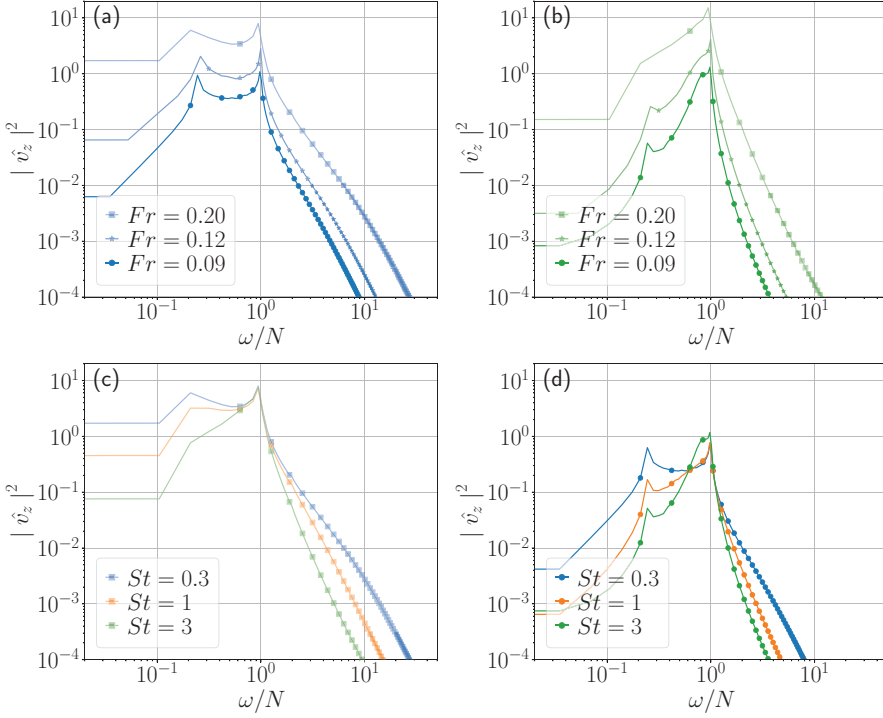


FIG. 2. Power spectrum of the particles' vertical velocity from the model in Eq. (13) for different values of Fr and (a) $St = 0.3$ and (b) $St = 3$. Note the decrease in the power with decreasing Fr . Same for different values of St and for (c) $Fr = 0.20$ and (d) $Fr = 0.09$. The value of St changes the frequency of the main peak and the amplitude of the secondary peak.

spectrum [2,47]. In other words, this process results in \dot{z}_{wav} being a random variable compatible with that spectrum.

Figure 2 shows the power spectrum obtained after integrating Eq. (13) using this random process as the forcing, for different values of the Brunt-Väisälä frequency and the Stokes number. Spectra are qualitatively similar to those shown in Fig. 1. The spectra display two peaks, the main one close to $\omega \approx N$. At fixed Fr , increasing St results in a broadening of this peak towards smaller frequencies. The second peak at lower frequencies has increasing amplitude with decreasing Fr , and appears at similar frequencies as those in Fig. 1. It is natural to ask whether these peaks are caused by the forcing or by the damped oscillations of the particles. Changing the forcing while still maintaining the Garrett-Munk spectrum for u_z (e.g., setting $f_{\text{wav}} = \ddot{z}_{\text{wav}}$) yields the same qualitative results, which indicates the peaks in the spectra are partially associated to the damped dynamics of the particles. Also, changing the lower cut-off frequency in Eq. (14) (i.e., the choice of $\omega > N/4$) has no effect on the position of the main peak close to $\omega \approx N$ and on the spectrum at higher frequencies, although it has a small effect on the position of the second peak at lower frequencies.

Equation (13) can be also rewritten in terms of the vertical slip velocity, $v_{\text{slip}} = u_z - v_z$. Taking $y = z - z_{\text{wav}}$, Eq. (13) results in the homogeneous damped harmonic oscillator equation. As before, the resulting oscillation frequency is $\Omega^2 = 2N^2/3 - (2\tau_p)^{-2}$, with exponential decay rate $(2\tau_p)^{-1}$. Noting that $\dot{y} = v_{\text{slip}}$, we can expect the vertical slip velocity of the particles to display overdamped or underdamped oscillations depending on the sign of Ω^2 . Figure 3 shows v_{slip} for particles in the numerical simulations with $St = 3$ ($\tau_p = 0.235T_0$) in a stratified fluid with $N = 12/T_0$ and $8/T_0$. Both cases have $\Omega^2 > 0$, and dynamics reminiscent of underdamped oscillations can be identified in the time series. The power spectrum of v_{slip} for multiple simulations, also shown in Fig. 3, shows

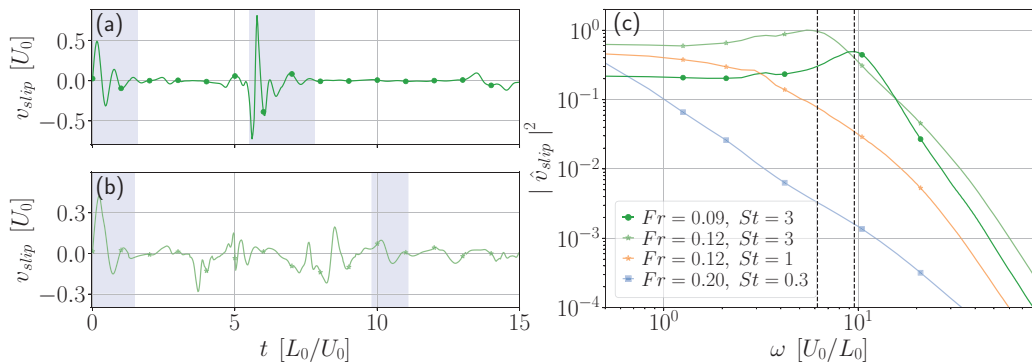


FIG. 3. Time series of the vertical slip velocity for two particles with $St = 3$ in stratified fluids with (a) $Fr = 0.09$ and (b) $Fr = 0.12$. Shaded regions indicate motions reminiscent of underdamped oscillations. (c) Power spectrum of the particles' vertical slip velocity, for different values of Fr and St (see inset). Overdamped particles show no peak in the spectrum, while underdamped particles display a peak at frequencies indicated by the vertical dashed lines.

peaks at the expected value of Ω in these two simulations, and no peaks in the other simulations with $\Omega^2 < 0$. Thus, the dynamics of the individual particles is compatible with randomly forced damped oscillators, with both τ_p and N controlling the particles' dynamical regime.

V. VERTICAL DISPERSION OF INERTIAL PARTICLES

Stratification limits vertical motions of the particles, strongly impairing vertical dispersion, and resulting in saturation of the mean squared vertical displacements of the particles with time. Linear models predict this saturation to take place after $t \approx 2\pi/N$, as particle displacements get constrained vertically by stratification, resulting in oscillatory motions around the neutrally buoyant equilibrium [48]. This was confirmed in numerical simulations with moderate Rb [11]. Later, studies of vertical dispersion of tracers in stably stratified flows [18,19], and of small neutrally buoyant particles with small St [20], explicitly confirmed the saturation of the mean squared vertical dispersion. For neutrally buoyant inertial particles the saturation was found to be faster and stronger than for Lagrangian tracers [20].

Figure 4 shows the particles' mean squared vertical displacement in the simulations, $\langle \delta z^2(t) \rangle = \langle [z_i(t) - z_i(0)]^2 \rangle_i$ (where the subindex i indicates the average is computed over all particle labels), for different values of Fr and St . Time is normalized by $2\pi/N$ and $\langle \delta z^2(t) \rangle$ is normalized by $(U_z/N)^2$, where U_z is the Eulerian r.m.s. fluid vertical velocity in the turbulent steady state. With this normalization curves collapse from $t = 0$ to $t \lesssim 2\pi/N$, in a time interval with ballistic behavior. The end of this regime at a time proportional to the wave period $2\pi/N$, instead of the Lagrangian eddy turnover time, indicates that the rapid early vertical displacements are caused by the inertial particles following the inertial waves. Note also that there is more overshooting in the vertical displacements (i.e., $\langle \delta z^2 \rangle$ reaches larger values in its maximum at the end of this ballistic stage) as St (and particle inertia) increases. After this maximum, inertial particles oscillate around their equilibrium position, displaying a plateau in the mean squared vertical displacements, as also reported in Ref. [20]. The amplitude of the plateau is weakly dependent on St , and depends strongly on Fr (see Ref. [38] for a movie showing the vertical displacements of the three different types of particles when $N = 4/T_0$, illustrating the confinement in vertical layers). This is different from the case of tracers in stratified flows, which for sufficiently large Rb display some slow vertical dispersion at late times caused by turbulent eddies or by diffusion [19].

The confinement of particles around a layer can be also characterized using the probability density function (PDF) of finding a particle at a given height, either in terms of z , or of the density

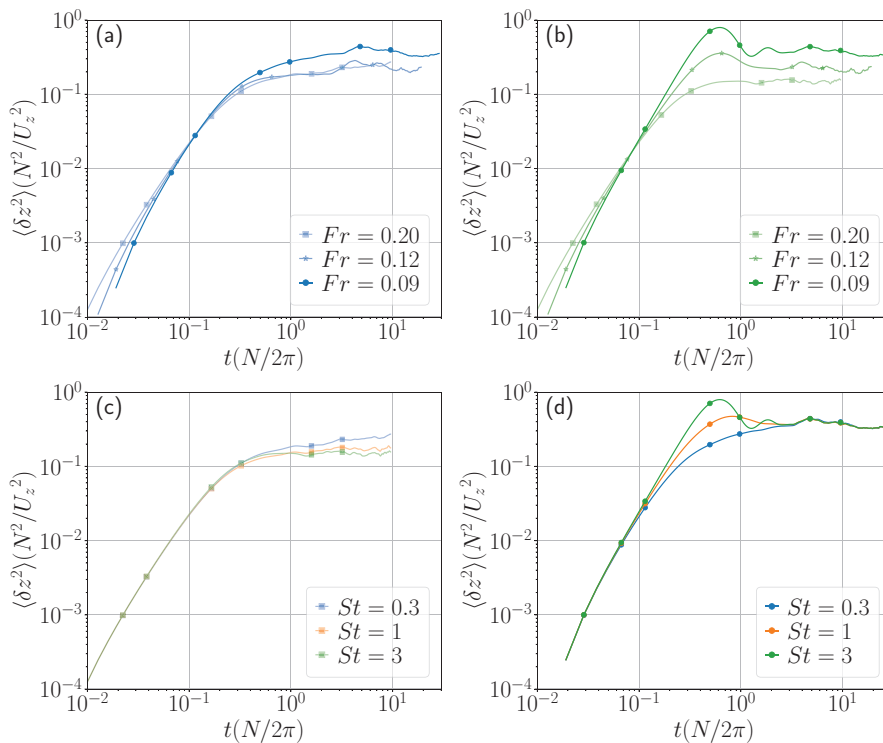


FIG. 4. Mean squared vertical displacements $\langle \delta z^2 \rangle$ as a function of time for different values of Fr and for (a) $St = 0.3$ and (b) $St = 3$. Also, for different values of St and for (c) $Fr = 0.20$ and (d) $Fr = 0.09$. In all cases, δz^2 is normalized by U_z^2/N^2 , and time is normalized by $2\pi/N$.

at each particle position (i.e., of how far the particle is from the equilibrium isopycnal). Figure 5 shows the PDF of z for different Fr and St , centered by the mean value and normalized by the dispersion. It is interesting to note that as the value of Fr decreases, the asymmetry in the tail of the PDF increases. While we cannot discard a single large event as the cause of this asymmetry, long-lived skewed PDFs of the fluid vertical velocity have been reported in Ref. [49]. They can be associated to the occurrence of extreme vertical drafts in stably stratified flows for values of Fr in the range ≈ 0.05 to 0.30 [50], which can cause more frequent and larger vertical wanderings of the particles. Figure 6 shows the same PDFs but in terms of the rescaled density fluctuations ζ at the particles positions, also centered by the mean value and normalized by the dispersion. These PDFs are closer to Gaussian and less sensitive to St but still display asymmetric tails for $Fr = 0.09$.

From Fig. 4 it seems apparent that particles are confined in a narrower layer as Fr decreases, but this is not evident from Figs. 5 and 6 as the PDFs in those figures are normalized by their standard deviations. Figure 7 shows the standard deviations in z and ζ of the particles, σ_z and σ_ζ , respectively, as a function of Fr^{-1} for all St considered. Note that both deviations (which can be considered as a measure of the height of the confinement layer) are a fraction of L_b , and decrease with decreasing Fr . The behavior of σ_z depends also on St for weak stratification. Sozza *et al.* [51] observed that for large values of Fr , σ_z was larger for larger τ_p (i.e., larger St), the opposite behavior of what is found here. The effect in Ref. [51] resulted from particles with more inertia being suspended from the equilibrium position for longer. Here, the mean winds in the shear layer of the Taylor-Green flow result in a different effect. Particles with more inertia are less affected by rapid vertical motions, following instead the slower horizontal motions and averaging over the vertical fluctuations as they move (see the movie in Ref. [38]). This is evident in Fig. 1, where it is observed that for the case with

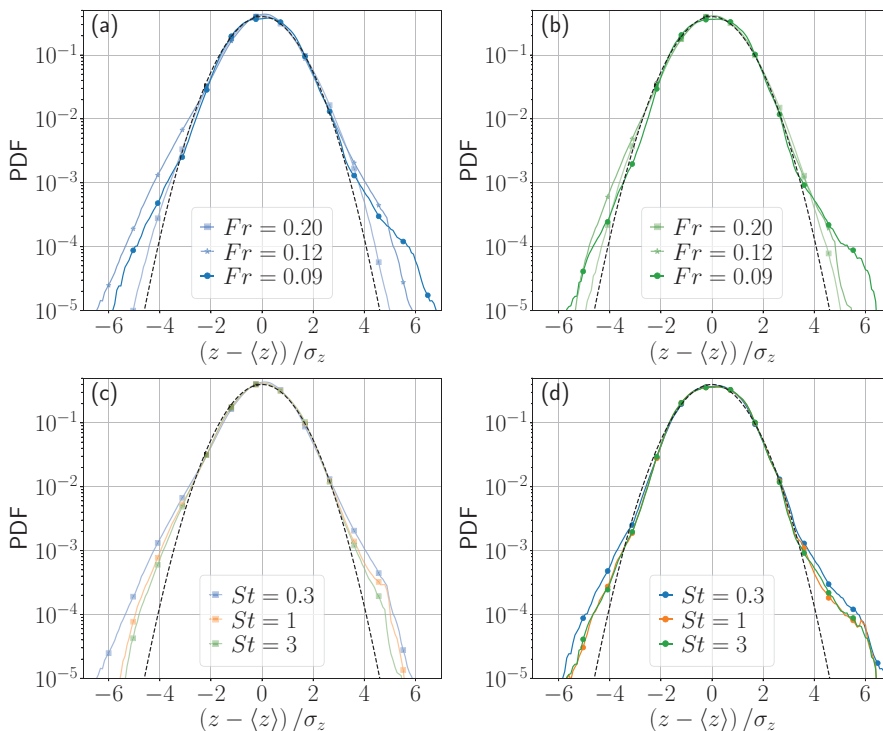


FIG. 5. Normalized probability density functions (PDFs) of the z position of particles for different values of Fr and (a) $St = 0.3$ and (b) $St = 3$. Same for different values of St and (c) $Fr = 0.20$ and (d) $Fr = 0.09$. The black dashed lines indicate as a reference a normal distribution.

$St = 0.3$ the main peak of the power spectrum of the particles' vertical velocity is above unity, while for the case with $St = 3$ the peak is below unity. This confirms that particles with lower inertia are more affected by the fluid vertical displacements, while particles with larger inertia are less affected by them. Thus, the behavior of σ_z with St for larger Fr is not universal, and probably dependent on the flow. However, the situation is different for σ_z , as shown in Fig. 4(b): $\sigma_z / (L_b N) = \sigma_z / U$ seems to depend linearly on Fr^{-1} , and is independent of St , at least in the range of parameters considered. Note this amounts to the dispersion of the particles around the isopycnal decreasing linearly with increasing Brunt-Väisälä frequency.

VI. CLUSTER FORMATION AND VORONOÏ TESSELLATION

The vertical confinement of particles has consequences for cluster formation. Clustering of particles has been reported in oceanic flows. As an example, phytoplankton can form complex structures with sizes of the order of the kilometer [46,52], also forming thin layers at depths that correlate with regions of strong gradients in fluid density and vertical shear, which tend to occur at the bottom of the mixed layer [53]. Another known case is that of sargassum, a type of seaweed that serves as habitat for marine fauna, but which can carry high levels of arsenic and heavy metals, causing major problems when decomposing near coastal lines [33,54]. To quantify clustering in our simulations we use Voronoï tessellation. Tessellations have been shown to be useful to characterize preferential concentration of particles, see, e.g., Refs. [6,55–59], with the standard deviation of the Voronoï cell volumes or areas being associated to the amount of clustering [23,56,57]. For heavy particles in stratified turbulence, clustering has also been studied using radial distribution

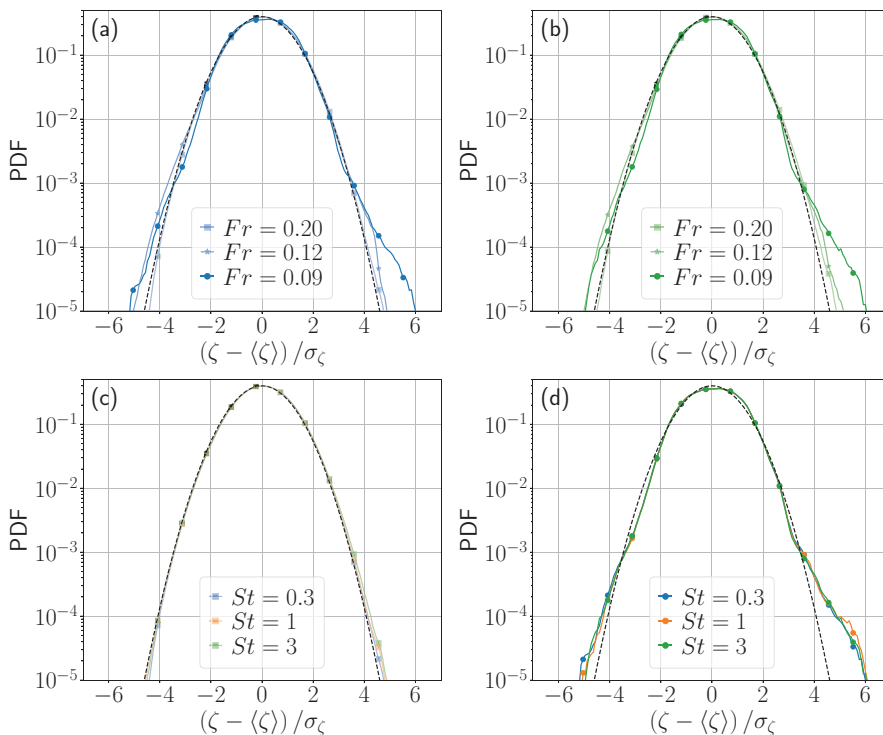


FIG. 6. Normalized PDFs of the rescaled density fluctuations ζ at the particles positions, in simulations with different Fr and (a) $St = 0.3$ and (b) $St = 3$. Same for particles with different St in flows with (c) $Fr = 0.20$ and (d) $Fr = 0.09$. Black dashed lines indicate a normal distribution.

functions [60], which give the ratio of the number of particle pairs found at a given separation to the expected number of pairs if particles are uniformly distributed. A Voronoi tessellation assigns a cell to each particle, so that each point in that cell is closer to that particle than to any other particle. Large tessellation cells correspond to voids (i.e., regions with far apart particles), while small cells correspond to clustered particles. While in the case of homogeneous and isotropic turbulence both three-dimensional (3D) and two-dimensional (2D) tessellations have been used, here we restrict ourselves to 2D tessellation as most of the particles remain in the thin layers discussed in the previous section. To that end, we project all particles into a plane, and consider only their x and y coordinates.

Figure 8 shows the PDFs of the normalized areas of the Voronoi cells, $\mathcal{A} = A/\langle A \rangle$, where A is the area of each cell. The figure also shows as a reference the PDF of a random Poisson process (RPP),

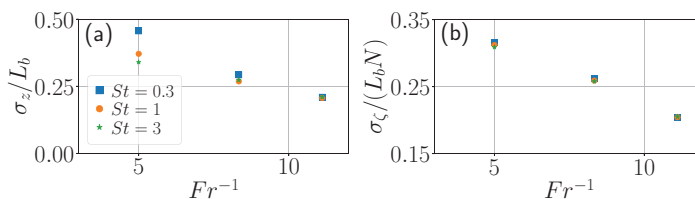


FIG. 7. Standard deviations of (a) the particles' positions in z normalized by the buoyancy length and (b) the fluid density variations at particles' positions, ζ , normalized by the buoyancy length and the Brunt-Väisälä frequency, as a function of the inverse of the Froude number.

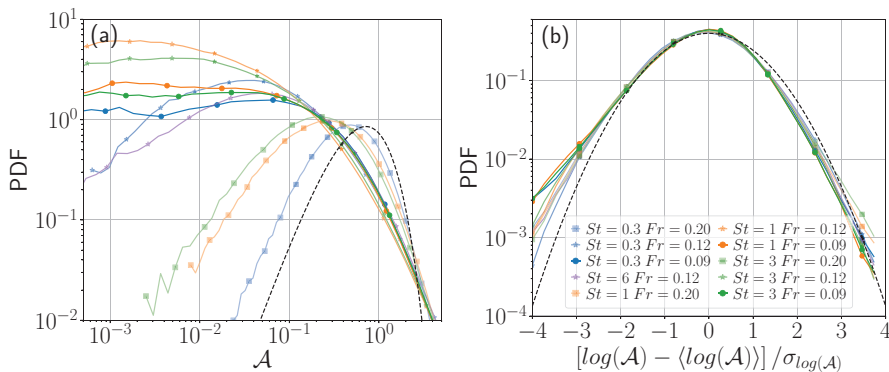


FIG. 8. (a) PDFs of the normalized Voronoi area \mathcal{A} for different values of Fr and St. (b) The logarithm (with base 10) of the volumes centered around their mean and normalized by their dispersion. The black dashed line indicates as a reference a random Poisson process, i.e., the PDF of randomly distributed particles. Note that, in addition to the simulations discussed so far, a new simulation with $St = 6$ and $Fr = 0.12$ is added in this figure to confirm that for fixed Fr, maximum clustering takes place for intermediate values of St.

which corresponds to particles randomly distributed in space [61,62]. The first crossing from the left between the PDFs and the RPP is often used to define clusters: an excess of smaller cells are an indication of a spatial accumulation of particles in certain regions of the flow. Note that particles in the flow with $Fr = 0.20$ are closer to the RPP. This is to be expected, as small neutrally buoyant particles do not cluster in the limit of homogeneous and isotropic turbulence (i.e., in the limit of $Fr \rightarrow \infty$, see Ref. [29] for a numerical study of small neutrally buoyant particles in this regime and Ref. [27] for a laboratory study). More importantly, clustering increases rapidly as Fr is decreased. The strongest clustering is obtained for intermediate stratification at $Fr = 0.12$ and $St = 1$. This indicates that although the increase in stratification is favorable for cluster formation, its effect is not monotonous with Fr, or with St. To confirm that maximum clustering occurs in the vicinity of $St = 1$, a new simulation (not discussed before) is shown only in Fig. 8, with $St = 6$ and $Fr = 0.12$, which (even though for this St neglecting the Basset-Boussinesq force is less justified) displays less clustering and can be compared with the other particles with different values of St at the same Fr.

The clusters seem to form in regions of the flow with low vertical vorticity, thus resulting from centrifugal vortex expulsion [5]. To illustrate this Fig. 9 shows the Voronoi areas of a random subset of 10^4 particles with $St = 0.3$, in the three simulations with $Fr = 0.20, 0.12$, and 0.09 . Red regions in Figs. 9(a), 9(b), and 9(c) correspond to cells larger than the average (voids), and blue areas to cells smaller than the average (clusters). A movie with the time evolution of the particles in the case with $Fr = 0.12$ can be seen in Ref. [38]. Figures 9(d), 9(e), and 9(f) show the squared vertical vorticity ω_z^2 averaged in each Voronoi cell, and normalized by its mean value (as a reference, the bottom panels show the same vorticity at full resolution, i.e., not coarse-grained). Note there is some correlation between these panels: regions of low vorticity seem to correspond to smaller Voronoi areas, specially for small Fr. A similar correlation between clusters and low vorticity regions was reported before for the case of heavy particles in stratified turbulence in Ref. [60]. We also use the distance correlation,

$$dCor_{XY} = \frac{\mu_{XY}}{(\mu_{XX}\mu_{YY})^{1/2}}, \quad (15)$$

where μ_{XY} , μ_{XX} , and μ_{YY} are, respectively, the correlation and autocorrelation functions between variables X and Y as defined in Refs. [63,64]. This coefficient is expected to give a better estimation of correlation than the Pearson correlation coefficient when the relation between variables is not

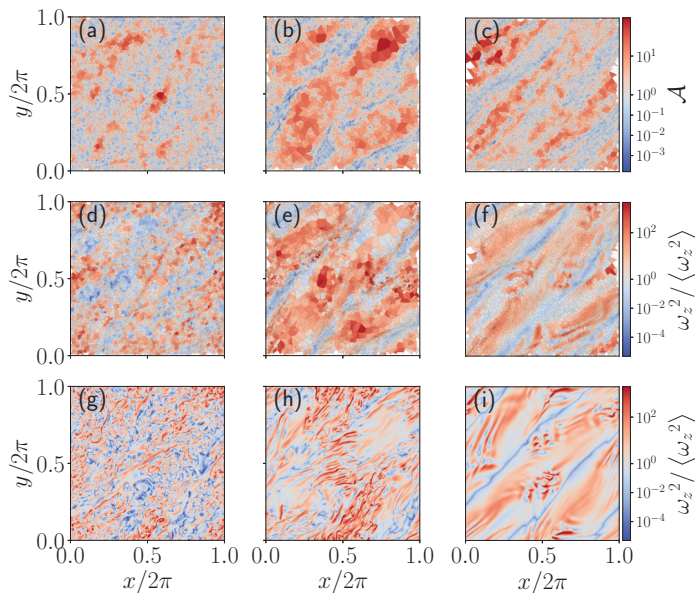


FIG. 9. Comparison between Voronoi particles' areas \mathcal{A} and the flow vertical vorticity. The first row shows the Voronoi areas of 10^4 particles with $St = 0.3$, for (a) $Fr = 0.20$, (b) 0.12 , and (c) 0.09 . In the middle row, the normalized squared flow vertical vorticity ω_z^2 is coarse-grained to the Voronoi areas, for the same three values of Fr , respectively, in (d), (e), and (f). The bottom row shows the full resolution ω_z^2 for the three values of Fr in (g), (h), and (i).

necessarily linear. We obtain $dCor_{\mathcal{A}\omega_z^2} = 0.20, 0.25, \text{ and } 0.31$, respectively, for $Fr = 0.20, 0.12$, and 0.09 . The correlation increases with stratification.

Figure 10 further confirms this correlation by showing joint PDFs of \mathcal{A} vs ω_z^2 for all simulations and particles. In the panels of Fig. 10 the vertical dashed lines indicate, from left to right, the first and second crossings of the PDFs of \mathcal{A} with the RPP (i.e., the values of \mathcal{A} below and above which cells correspond, respectively, to clustered particles and to voids). Particles in voids tend to be in regions of larger vorticity, and the correlation is more clear as Fr decreases. As a reference, we indicate different slopes with straight lines. Note that for strong stratification ($Fr = 0.12$), the shape of the PDFs becomes almost insensitive to the value of St . Overall, a correlation between large Voronoi areas and large vorticity appears independently of the Stokes number in the strongly stratified cases.

VII. CONCLUSIONS

We presented a numerical study of the transport and spatial accumulation of light neutrally buoyant inertial particles in stably stratified turbulent flows, using the Maxey-Riley equation for small particles. We showed that in the stratified case, the equation can be written as the equation of a driven damped oscillator, with two regimes controlled by the inverse squared particle response time, τ_p^{-2} , and the flow Brunt-Väisälä frequency, N . When the former is larger particles are overdamped, while when the latter is larger particles are underdamped. This results in the appearance of two peaks in the power spectrum of the particles' vertical velocity, the main peak with frequency $\Omega \approx [2N^2/3 - (2\tau_p)^{-2}]^{-1/2}$.

As observed in previous studies of light and heavy particles in stably stratified turbulence [20,60], the vertical dispersion of particles is strongly confined in layers. The width of this layer depends on the Stokes and Froude numbers. However, when studied in terms of density isopycnals, the width

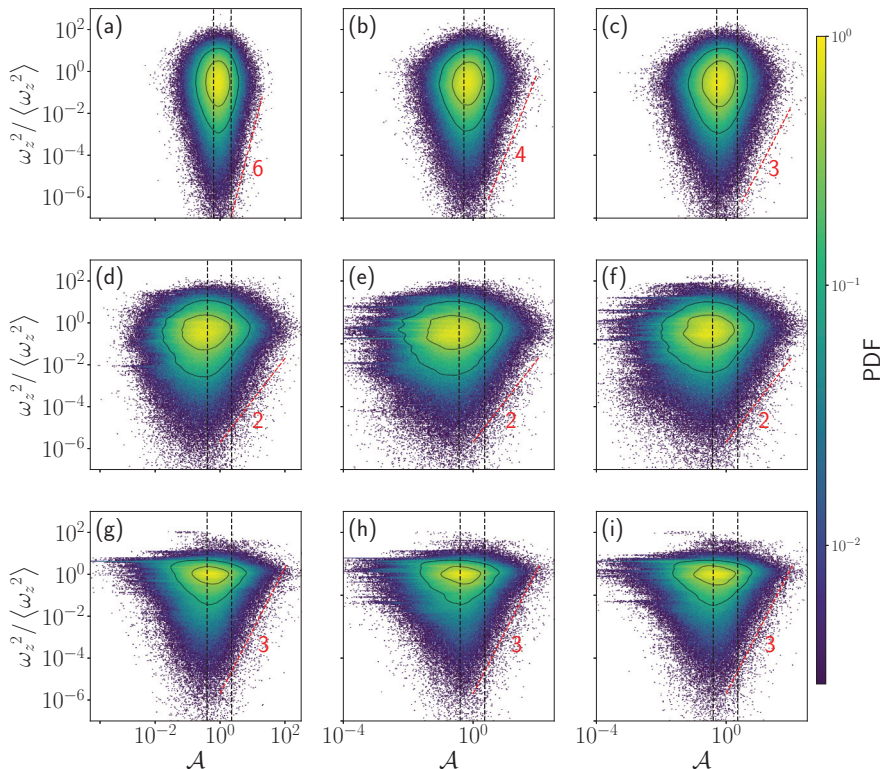


FIG. 10. Joint PDFs of \mathcal{A} and ω_z^2 . From left to right, $St = 0.3, 1,$ and 3 . From top to bottom, $Fr = 0.20, 0.12,$ and $Fr = 0.09$. As an example, panel (a) has $St = 0.3$ and $Fr = 0.20$, (b) has $St = 1$ and $Fr = 0.20$, (c) has $St = 3$ and $Fr = 0.20$, (d) has $St = 0.3$ and $Fr = 0.12$, and so on. Vertical dashed lines, from left to right, indicate, respectively, the first and second crossings of the PDF of \mathcal{A} with the RPP. Several slopes are indicated with red dashed curves only as a reference.

becomes independent of the particles' Stokes number (at least, in the range of parameters considered in this study), and varies with the Brunt-Väisälä frequency.

This vertical confinement also has a strong impact in the clustering of particles, and in the physical mechanism behind cluster formation. We showed that a two-dimensional Voronoi tessellation can be used to study clusters; previous studies using other methods for vertically confined particles can be seen in Refs. [60,65]. Our analysis indicates that in sufficiently stratified flows the formation of clusters is governed by centrifugal vortex expulsion, independently of whether the Stokes number is smaller or larger than unity. Moreover, clustering is strongly enhanced as stratification is increased, and this enhancement takes place also when only considering the two-dimensional positions of the particles, i.e., independently of the particles' vertical confinement. This result can be important to compute particle collisions and particle-turbulence interactions in atmospheric problems [66,67], and in oceanic flows where patches of phytoplankton and of nutrients are commonly observed [31,46,52]. The result is also reminiscent of observations of clustering in floaters in free surface flows, where the large-scale flow circulation can play an important role in particle accumulation [68].

ACKNOWLEDGMENTS

The authors acknowledge financial support from UBACyT Grant No. 20020170100508BA and PICT Grant No. 2018-4298. This research was supported in part by the National Science Foundation under Grant No. NSF PHY-1748958.

-
- [1] J. Wyngaard, Turbulence in the atmosphere, *Annu. Rev. Fluid Mech.* **24**, 205 (1992).
- [2] E. D'Asaro and R.-C. Lien, Lagrangian measurements of waves and turbulence in stratified flows, *J. Phys. Oceanogr.* **30**, 641 (2000).
- [3] T. Watanabe, J. Riley, S. de Bruyn Kops, P. Diamessis, and Q. Zhou, Turbulent/nonturbulent interfaces in wakes in stably stratified fluids, *J. Fluid Mech.* **797**, R1 (2016).
- [4] G. Amir, N. Bar, A. Eidelman, T. Elperin, N. Kleeorin, and I. Rogachevskii, Turbulent thermal diffusion in strongly stratified turbulence: Theory and experiments, *Phys. Rev. Fluids* **2**, 064605 (2017).
- [5] M. Maxey and J. Riley, Equation of motion for a small rigid sphere in a nonuniform flow, *Phys. Fluids* **26**, 883 (1983).
- [6] M. Obligado, A. Cartellier, and M. Bourgoïn, Experimental detection of superclusters of water droplets in homogeneous isotropic turbulence, *Europhys. Lett.* **112**, 54004 (2015).
- [7] V. Tavanashad, A. Passalacqua, and S. Subramaniam, Particle-resolved simulation of freely evolving particle suspensions: Flow physics and modeling, *Int. J. Multiphase Flow* **135**, 103533 (2021).
- [8] P. Wagner, S. Rühls, F. U. Schwarzkopf, I. M. Koszalka, and A. Biastoch, Can Lagrangian tracking simulate tracer spreading in a high-resolution ocean general circulation model? *J. Phys. Oceanogr.* **49**, 1141 (2019).
- [9] T. Palmer, Stochastic weather and climate models, *Nat. Rev. Phys.* **1**, 463 (2019).
- [10] F. J. Beron-Vera, M. J. Olascoaga, and P. Miron, Building a Maxey-Riley framework for surface ocean inertial particle dynamics, *Phys. Fluids* **31**, 096602 (2019).
- [11] G. B. E. Lindborg, Vertical dispersion by stratified turbulence, *J. Fluid Mech.* **614**, 303 (2008).
- [12] R. Marino, P. D. Mininni, D. L. Rosenberg, and A. Pouquet, Large-scale anisotropy in stably stratified rotating flows, *Phys. Rev. E* **90**, 023018 (2014).
- [13] G. D. Portwood, S. M. de Bruyn Kops, and C. P. Caulfield, Asymptotic Dynamics of High Dynamic Range Stratified Turbulence, *Phys. Rev. Lett.* **122**, 194504 (2019).
- [14] L. Smith and F. Waleffe, Generation of slow large scales in forced rotating stratified turbulence, *J. Fluid Mech.* **451**, 145 (2002).
- [15] M. L. Waite, Stratified turbulence at the buoyancy scale, *Phys. Fluids* **23**, 066602 (2011).
- [16] A. Maffioli, Vertical spectra of stratified turbulence at large horizontal scales, *Phys. Rev. Fluids* **2**, 104802 (2017).
- [17] J. Riley, Dynamics of turbulence strongly influenced by buoyancy, *Phys. Fluids* **15**, 2047 (2003).
- [18] M. van Aartrijk, H. J. H. Clercx, and K. B. Winters, Single-particle, particle-pair, and multiparticle dispersion of fluid particles in forced stably stratified turbulence, *Phys. Fluids* **20**, 025104 (2008).
- [19] N. E. Sujovolsky and P. D. Mininni, Vertical dispersion of Lagrangian tracers in fully developed stably stratified turbulence, *Phys. Rev. Fluids* **4**, 014503 (2019).
- [20] M. van Aartrijk and H. J. H. Clercx, Vertical dispersion of light inertial particles in stably stratified turbulence: The influence of the Basset force, *Phys. Fluids* **22**, 013301 (2010).
- [21] A. Sozza, F. Lillo, S. Musacchio, and G. Boffetta, Large-scale confinement and small-scale clustering of floating particles in stratified turbulence, *Phys. Rev. Fluids* **1**, 052401 (2016).
- [22] S. Goto and J. C. Vassilicos, Sweep-Stick Mechanism of Heavy Particle Clustering in Fluid Turbulence, *Phys. Rev. Lett.* **100**, 054503 (2008).
- [23] M. Obligado, T. Teitelbaum, A. Cartellier, P. Mininni, and M. Bourgoïn, Preferential concentration of heavy particles in turbulence, *J. Turbul.* **15**, 293 (2014).
- [24] A. D. Bragg, P. J. Ireland, and L. R. Collins, Mechanisms for the clustering of inertial particles in the inertial range of isotropic turbulence, *Phys. Rev. E* **92**, 023029 (2015).
- [25] J. Tom and A. D. Bragg, Multiscale preferential sweeping of particles settling in turbulence, *J. Fluid Mech.* **871**, 244 (2019).
- [26] H. Homann and J. Bec, Finite-size effects in the dynamics of neutrally buoyant particles in turbulent flow, *J. Fluid Mech.* **651**, 81 (2010).
- [27] L. Fiabane, R. Zimmermann, R. Volk, J. F. Pinton, and M. Bourgoïn, Clustering of finite-size particles in turbulence, *Phys. Rev. E* **86**, 035301(R) (2012).
- [28] S. Angriman, P. D. Mininni, and P. J. Cobelli, Velocity and acceleration statistics in particle-laden turbulent swirling flows, *Phys. Rev. Fluids* **5**, 064605 (2020).

- [29] C. Reartes and P. D. Mininni, Settling and clustering of particles of moderate mass density in turbulence, *Phys. Rev. Fluids* **6**, 114304 (2021).
- [30] I. McCave, Size spectra and aggregation of suspended particles in the deep ocean, *Deep Sea Res. Part A* **31**, 329 (1984).
- [31] K. D. Squires and H. Yamazaki, Preferential concentration of marine particles in isotropic turbulence, *Deep Sea Res. Part A* **42**, 1989 (1995).
- [32] E. Acevedo-Trejos, G. Brandt, J. Bruggeman, and A. Merico, Mechanisms shaping size structure and functional diversity of phytoplankton communities in the ocean, *Sci. Rep.* **5**, 8918 (2015).
- [33] F. J. Beron-Vera and P. Miron, A minimal Maxey-Riley model for the drift of sargassum rafts, *J. Fluid Mech.* **904**, A8 (2020).
- [34] L. M. Russell, A. Sorooshian, J. H. Seinfeld, B. A. Albrecht, A. Nenes, L. Ahlm, Y.-C. Chen, M. Coggon, J. S. Craven, R. C. Flagan *et al.*, Eastern Pacific emitted aerosol cloud experiment, *Bull. Am. Meteorol. Soc.* **94**, 709 (2013).
- [35] J. N. Moum, Energy-containing scales of turbulence in the ocean thermocline, *J. Geophys. Res.* **101**, 14095 (1996).
- [36] G. Ivey, K. Winters, and J. Koseff, Density stratification, turbulence, but how much mixing? *Annu. Rev. Fluid Mech.* **40**, 169 (2008).
- [37] P. Clark di Leoni and P. D. Mininni, Absorption of waves by large-scale winds in stratified turbulence, *Phys. Rev. E* **91**, 033015 (2015).
- [38] See Supplemental Material at <http://link.aps.org/supplemental/10.1103/PhysRevFluids.8.054501> for movies showing the early development of a mean horizontal wind in the shear layer of the Taylor-Green flow, the vertical dispersion of the different particles in the simulation with $NT_0 = 4$, and the horizontal dispersion of particles with $St = 1$ in the simulation with $NT_0 = 8$.
- [39] P. Mininni, D. Rosenberg, R. Reddy, and A. Pouquet, A hybrid MPI-openmp scheme for scalable parallel pseudospectral computations for fluid turbulence, *Parallel Comput.* **37**, 316 (2011).
- [40] P. Yeung and S. Pope, An algorithm for tracking fluid particles in numerical simulations of homogeneous turbulence, *J. Comput. Phys.* **79**, 373 (1988).
- [41] Y. Li, F. Ries, W. Leudesdorff, K. Nishad, A. Pati, C. Hasse, J. Janicka, S. Jakirlić, and A. Sadiki, Non-equilibrium wall functions for large eddy simulations of complex turbulent flows and heat transfer, *Int. J. Heat Fluid Flow* **88**, 108758 (2021).
- [42] S. Basu and A. A. Holtslag, Turbulent prandtl number and characteristic length scales in stably stratified flows: Steady-state analytical solutions, *Environ. Fluid Mech.* **21**, 1273 (2021).
- [43] D. Donzis and P. Yeung, Resolution effects and scaling in numerical simulations of passive scalar mixing in turbulence, *Physica D* **239**, 1278 (2010).
- [44] M. Wan, S. Oughton, S. Servidio, and W. H. Matthaeus, On the accuracy of simulations of turbulence, *Phys. Plasmas* **17**, 082308 (2010).
- [45] G. K. Vallis, *Atmospheric and Oceanic Fluid Dynamics* (Cambridge University Press, Cambridge, UK, 2017)
- [46] W. M. Durham, E. Climent, M. Barry, F. D. Lillo, G. Boffetta, M. Cencini, and R. Stocker, Turbulence drives microscale patches of motile phytoplankton, *Nat. Commun.* **4**, 2148 (2013).
- [47] E. D'Asaro, R. C. Lien, and F. Henyey, High-frequency internal waves on the oregon continental shelf, *J. Phys. Oceanogr.* **37**, 1956 (2007).
- [48] F. Nicolleau and J. C. Vassilicos, Turbulent diffusion in stably stratified nondecaying turbulence, *J. Fluid Mech.* **410**, 123 (2000).
- [49] C. Rorai, P. D. Mininni, and A. Pouquet, Turbulence comes in bursts in stably stratified flows, *Phys. Rev. E* **89**, 043002 (2014).
- [50] F. Feraco, R. Marino, A. Pumir, L. Primavera, P. D. Mininni, A. Pouquet, and D. Rosenberg, Vertical drafts and mixing in stratified turbulence: Sharp transition with Froude number, *Europhys. Lett.* **123**, 44002 (2018).
- [51] A. Sozza, F. De Lillo, and G. Boffetta, Inertial floaters in stratified turbulence, *Europhys. Lett.* **121**, 14002 (2018).

- [52] A. Martin, Phytoplankton patchiness: The role of lateral stirring and mixing, *Prog. Oceanogr.* **57**, 125 (2003).
- [53] T. M. S. Johnston and D. L. Rudnick, Observations of the transition layer, *J. Phys. Oceanogr.* **39**, 780 (2009).
- [54] F. Andrade-Canto, F. Beron-Vera, G. Goni, D. Karrasch, M. Olascoaga, and J. Triñanes, Carriers of sargassum and mechanism for coastal inundation in the caribbean sea, *Phys. Fluids* **34**, 016602 (2022).
- [55] F. Pugliese and P. Dmitruk, Test particle energization of heavy ions in magnetohydrodynamic turbulence, *Astrophys. J.* **929**, 4 (2022).
- [56] R. Monchaux, M. Bourgoïn, and A. Cartellier, Preferential concentration of heavy particles: A Voronoï analysis, *Phys. Fluids* **22**, 103304 (2010).
- [57] R. Monchaux, M. Bourgoïn, and A. Cartellier, Analyzing preferential concentration and clustering of inertial particles in turbulence, *Int. J. Multiphase Flow* **40**, 1 (2012).
- [58] S. Sumbekova, A. Cartellier, A. Aliseda, and M. Bourgoïn, Preferential concentration of inertial sub-Kolmogorov particles: The roles of mass loading of particles, stokes numbers, and reynolds numbers, *Phys. Rev. Fluids* **2**, 024302 (2017).
- [59] M. Obligado, A. Cartellier, A. Aliseda, T. Calmant, and N. de Palma, Study on preferential concentration of inertial particles in homogeneous isotropic turbulence via big-data techniques, *Phys. Rev. Fluids* **5**, 024303 (2020).
- [60] M. van Aartrijk and H. J. H. Clercx, Preferential Concentration of Heavy Particles in Stably Stratified Turbulence, *Phys. Rev. Lett.* **100**, 254501 (2008).
- [61] M. Tanemura, Statistical distributions of poisson Voronoï cells in two and three dimensions, *Forma* **18**, 221 (2003).
- [62] M. Uhlmann, Voronoï tessellation analysis of sets of randomly placed finite-size spheres, *Physica A* **555**, 124618 (2020).
- [63] G. J. Székely, M. L. Rizzo, and N. K. Bakirov, Measuring and testing dependence by correlation of distances, *Ann. Stat.* **35**, 2769 (2007).
- [64] D. Edelmann, T. F. Móri, and G. J. Székely, On relationships between the Pearson and the distance correlation coefficients, *Stat. Probab. Lett.* **169**, 108960 (2021).
- [65] M. De Pietro, M. A. T. van Hinsberg, L. Biferale, H. J. H. Clercx, P. Perlekar, and F. Toschi, Clustering of vertically constrained passive particles in homogeneous, isotropic turbulence, *Phys. Rev. E* **91**, 053002 (2015).
- [66] R. A. Shaw, W. C. Reade, L. R. Collins, and J. Verlinde, Preferential concentration of cloud droplets by turbulence: Effects on the early evolution of cumulus cloud droplet spectra, *J. Atmos. Sci.* **55**, 1965 (1998).
- [67] R. A. Shaw, Particle-turbulence interactions in atmospheric clouds, *Annu. Rev. Fluid Mech.* **35**, 183 (2003).
- [68] N. F. Del Grosso, L. M. Cappelletti, N. E. Sujovolsky, P. D. Mininni, and P. J. Cobelli, Statistics of single and multiple floaters in experiments of surface wave turbulence, *Phys. Rev. Fluids* **4**, 074805 (2019).